# CHAPTER 6

# Tribological behaviour of silicon carbide (SiC) and graphite (Gr) reinforced copper-based hybrid composite

## 6.1 Introduction

The chapter discusses the results of creating composites by the powder metallurgy technique, employing different weight percentages of silicon carbide (SiC) and graphite (Gr) particles. The copper composites underwent analysis using multiple methodologies to investigate the influence of varying weight percentages of SiC and graphite particles on the microstructure, physical characteristics, and mechanical properties of the composites. The results and their ramifications are presented and analysed. The dry sliding friction and wear characteristics are examined using the conventional pin-on-disc apparatus. Both the standard load and the velocity of sliding have remained constant. The test utilises a counter face made of EN31 hardened steel. The morphology, distribution, and constitution of reinforcements exert a significant influence on the tribological characteristics of composite materials. The study investigates the tribological characteristics in relation to several factors, such as sliding distance, applied stress, sliding velocity, and the weight percentage of SiC and graphite. The worn surfaces of the composites were analysed using a Scanning Electron Microscope (SEM) that was connected to an Atomic Force Microscope (AFM) and an Energy Dispersive Spectroscopy (EDS) system.

## 6.2. Copper-based (Cu-Gr-SiC) hybrid composite

### 6.2.1 microstructural analysis

The existence and distribution of reinforcements in the matrix and their bonding with the matrix phases are made clear by the microstructural analysis. The SEM micrographs of the S1, S2, S3, and S4 are shown in Figures 6.1(a) through (d), respectively. The scanning electron micrograph of the unreinforced copper (S1) does not indicate the presence of any other elements; rather, it just displays a comparable type of grain structure, i.e., copper grains. On the other hand, as

illustrated in Figures 6.1(b) through (d), the microstructural analysis of the created hybrid composites (S2, S3, and S4) shows that the reinforcements are evenly distributed throughout the matrix. The uniform dispersion of reinforcements significantly influences the mechanical and tribological properties of composites made of the materials. Figures 6.1(c) and (d) depict the SEM micrographs of composites (S3 and S4), which showed a greater dispersion of graphite and SiC particles in the matrix phase as the weight percentage of reinforcement increased. Additionally, the SEM micrographs show that the composites with the reinforcement in the copper matrix are not fracturing. In the SEM micrographs, pores are sporadically visible and a rare aggregation of graphite and SiC particles at greater concentration is also seen.

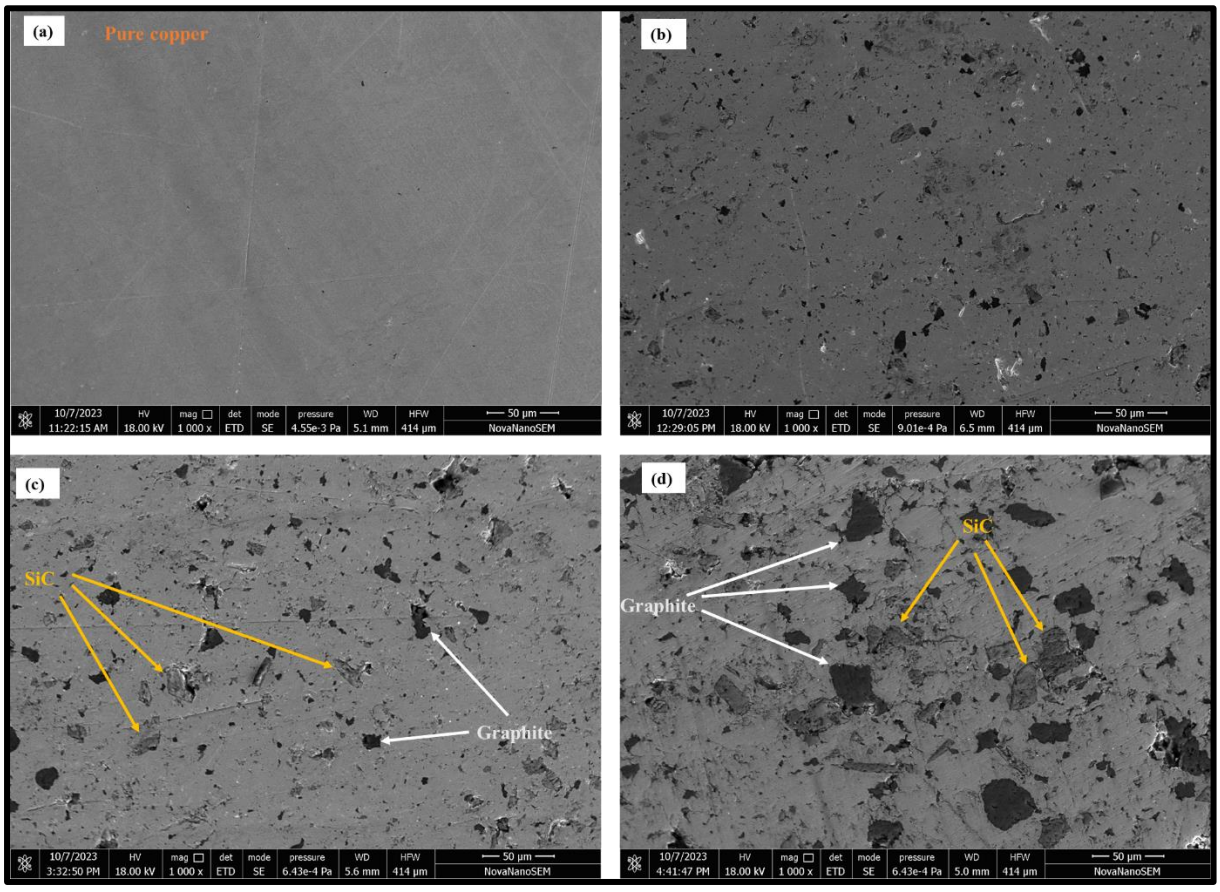


**Figure 6.1** SEM micrograph of the developed specimens (a) S1, (b) S2, (c) S3, and (d) S4

The absence of microcracks in the composites' SEM micrograph indicates enough interfacial strength or bonding between the matrix and the particles. However, it is challenging to tell the SiC and graphite particles apart with the unaided eye during the microstructural analysis because of their similar appearances. In order to strengthen the claim that reinforcing materials are present in the matrix for the SEM pictures, elemental colour mapping using Energy Dispersive Spectroscopy (EDS) is also carried out for the created composite materials, as illustrated in Figure 6.2. As the proportion of SiC and graphite particles in the composite increased, correspondingly increased, the elemental mapping appears for elements Si and C. Figure 6.3 displays the EDS spectra of the produced composites (S1), (S2), and (S4) specimens along with their concentration tables. As seen in Figure 6.3, the concentration table of composites demonstrates the presence of each element, including copper (Cu), chromium (Cr), silicon (Si), and carbon(C).

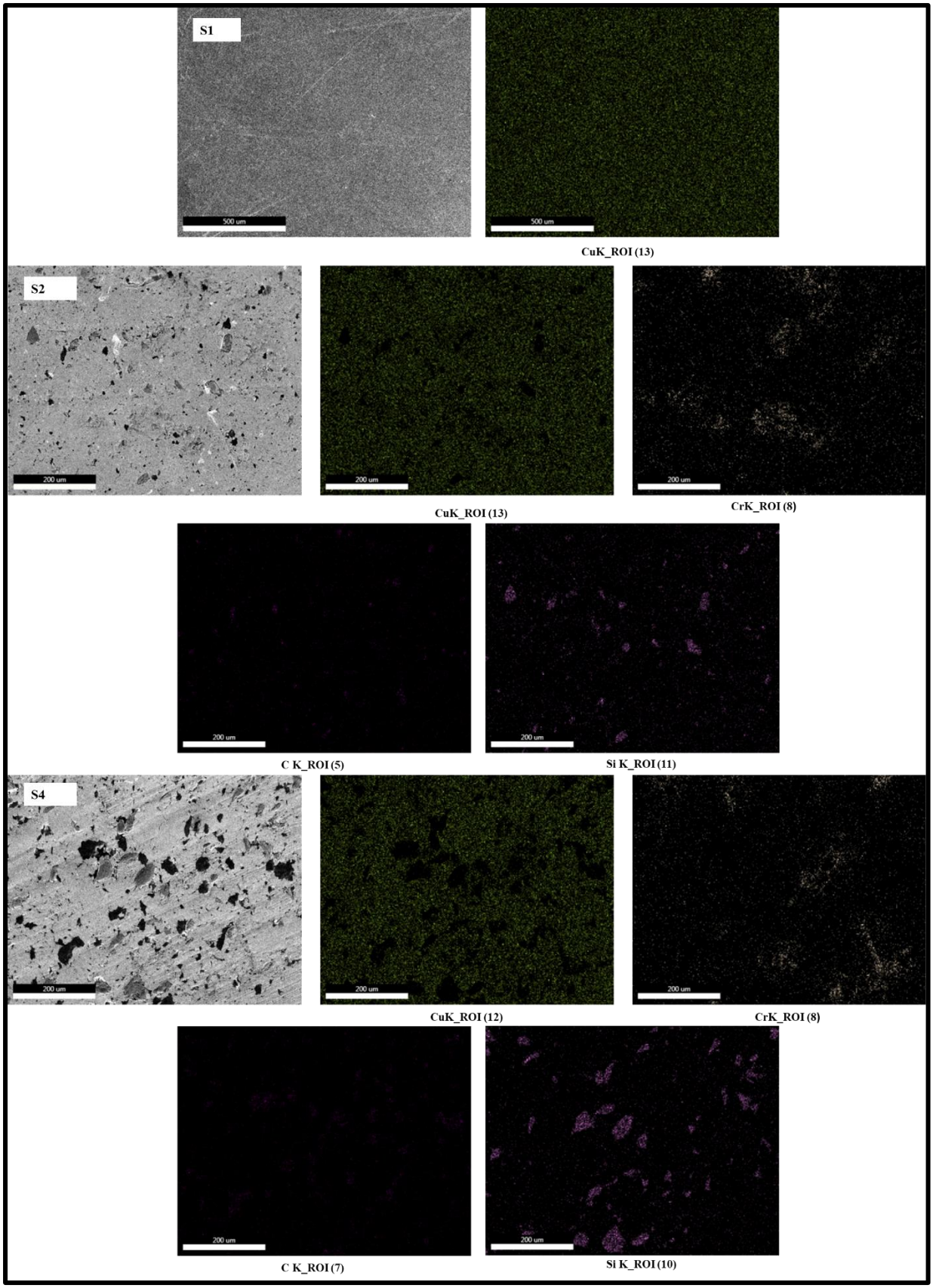


**Figure 6.2.** EDS Elemental color mapping of S1,S2 and S4 composite specimens

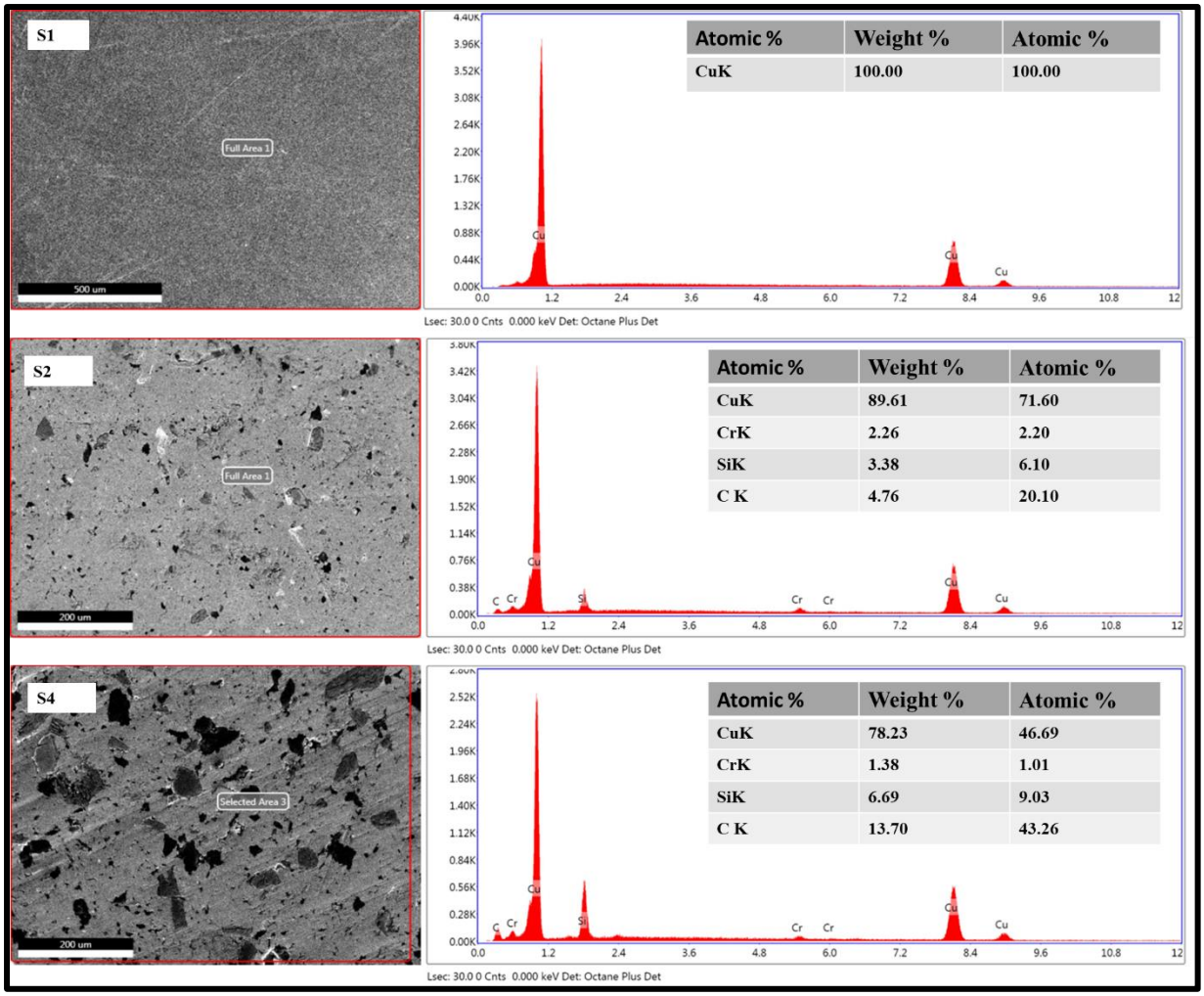


**Figure 6.3.** EDS spectrum of S1,S2 and S4 composite specimens

### 6.2.2 Physical and mechanical properties

The developed materials' porosity, hardness, theoretical density, and sintered (experimental) density are all detailed in Table 6.1. The table makes it abundantly evident that the theoretical and sintered densities of the composite specimens are lower than those of the unreinforced copper specimens. It is demonstrated by reinforcing lightweight elements in the copper matrix, such as SiC (3.21 g/cm3) and graphite (2.20 g/cm3). Additionally, it is noted that when the number of reinforcing particles in the matrix increases, the experimental and theoretical densities of the composites decrease.

| S. No. | Developed materials | Theoretical density ($g/cm^3$) | Sintered/experimental density ($g/cm^3$) | Porosity (%) | Hardness (Hv) |
|---|---|---|---|---|---|
| **1** | S1 | 8.96 | 8.43 ± 0.10 | 5.91 ± 0.11 | 56.5 ± 1 |
| **2** | S2 | 8.31 | 7.51 ± 0.10 | 9.62 ± 0.09 | 83.3 ± 15 |
| **3** | S3 | 7.78 | 6.81 ± 0.13 | 12.46 ± 0.13 | 93.6 ± 2.5 |
| **4** | S4 | 7.32 | 6.26 ± 0.15 | 14.48 ± 0.11 | 78.6 ± 1.2 |

**Table 6.1** Theoretical density, sintered (experimental) density, porosity, and hardness of the developed materials

The data indicates that the sintered or experimental density of composites reduces from 8.43 g/cm3 to 7.51 g/cm3 upon the addition of graphite and SiC with a total weight of 3 wt.% in the matrix. This decrease also occurs upon additional reinforcement addition in the copper matrix. Out of all the materials that have been produced, the composite (S4) has the lowest theoretical and experimental density. The size, kind, form, and composition of the particles as well as the substance itself all have an impact on the density of the material (Jamwal et al., 2020). According to Table 6.1, porosity in composites is higher than in their matrix and rises with an increase in the weight % of graphite and SiC content. It is ascribed to the homogeneous dispersion of boron carbide and graphite particles despite a tendency for agglomerates to develop at specific matrix sites, increasing porosity.

Table 6.1 displays the variation in Vickers hardness for all the materials that have been formed. The test findings demonstrate a substantial enhancement in the hardness of the composites when graphite and SiC are included into the copper metal matrix. An increase in the weight percentage of reinforcement in the created materials leads to an observed rise in hardness. Specifically, the hardness value increases from 56.5 to 83.3 when 3 wt.% of reinforcement is added, and from 56.5 to 93.6 when 6 wt.% of reinforcement is added to the copper matrix. The hardness value of S3 is 60.36% higher than that of the pure copper matrix. However, when a reinforcement of 9 wt.% is added to the copper matrix, the hardness value lowers to 78.6. This

value is lower than that of other composites but still higher than the hardness of the matrix alone. The enhanced hardness of the produced composites is attributed to incorporating SiC, which possesses a higher hardness level than the copper matrix(Bhowmik et al., n.d.).The excellent interfacial bonding between the SiC ceramic particle and the copper matrix, as well as the SiC particle's capacity to hinder dislocation motion, are also ascribed to it(Bharathi and kumar, 2023; Bharathi and Sampath Kumar, 2023). The decrease in hardness value seen in the composite, which contains 9 wt.% reinforcement in the matrix, can be related to the graphite's soft nature and its significant porosity(Meher and Chaira, 2017). The composite sample's hardness decrease, following the incorporation of 6wt.% reinforcement in the matrix, can be ascribed to the existence of graphite. Graphite is considerably softer than the Cu matrix, resulting in a lower hardness. Increased porosity in the composites causes the Gr-SiC particles to cluster together in the Cu matrix, resulting in a decrease in hardness for specimens with a Gr-SiC concentration above 6 wt.%.

### 6.2.3 Dry sliding friction and wear

#### 6.2.3.1 Effect of SiC and Gr content

Figure 6.4(a) shows how the wear rate of composite materials changes with different concentrations of reinforcement. The normal loads used were 10, 20, and 30 N, and the sliding speed was 2 m/s. The sliding distance covered was 2 km. The Figure demonstrates that as the amount of reinforcement increases, the rate of wear decreases in all of the materials studied, regardless of the applied loads of 10, 20, and 30 N. Nevertheless, the rate of wear escalates as the applied normal load increases for all of the materials that have been produced. S4 has wear rates that are 18%, 53.6%, and 62% lower than the wear rates of S3, S2, and S1, respectively. This means that S4 has the lowest wear rate among all the developed materials when subjected to a load of 30 N, a sliding speed of 2 m/s, and a sliding distance of 2 km. The enhanced wear resistance of the proposed composites is due to the incorporation of a higher weight percentage

of graphite. This graphite serves as a solid lubricant and greatly facilitates the surface interaction between the worn pin and counter disc (Radhika and Sam, 2019; Rajkumar and Aravindan, 2011). The wear resistance of the developed composites is enhanced by the inclusion of highly durable SiC particles. Additionally, the composites exhibit excellent interfacial bonding within the copper matrix, which prevents plastic deformation. Consequently, the composite materials become harder when harder SiC particles are added (Somani et al., 2019; Wu et al., 2024).

Figure 6.4(b) displays the change in coefficient of friction (COF) with varying weight percentages of reinforcement in a copper matrix. The experiment was conducted with normal loads of 10, 20, and 30 N, a sliding speed of 2 m/s, and a sliding distance of 2 km. Figure 6.4(b) demonstrates a decrease in COF values as the reinforcement content increases, regardless of the applied normal loads and sliding speed of 2 m/s. The coefficient of friction (COF) for the S1, S2, S3, and S4 specimens is seen to be 0.680, 0.601, 0.522, and 0.501, respectively, when a maximum normal load of 30 N is applied. The coefficient of friction (COF) of specimen S4 is approximately 35%, 30.2%, and 13.1% lower than that of specimens S1, S2, and S3, respectively, when a typical load of 30 N is applied. The increase in coefficient of friction (COF) observed in produced composites can be attributed to the addition of graphite, which possesses excellent lubricating properties, to the matrix. When the composites engage with the counter-rotating disc, the graphite particles will become visible. This interaction generates a lubricating surface between the mating surfaces, reducing further mating of the surfaces. The phenomena is possible because graphite possesses favourable qualities as a solid lubricant. The remark is corroborated by several literature publications that indicate a comparable result when there is a coexistence of rigid titanium carbide and graphite particles within a pliable matrix (Kumar et al., 2023; Rajkumar and Aravindan, 2011).

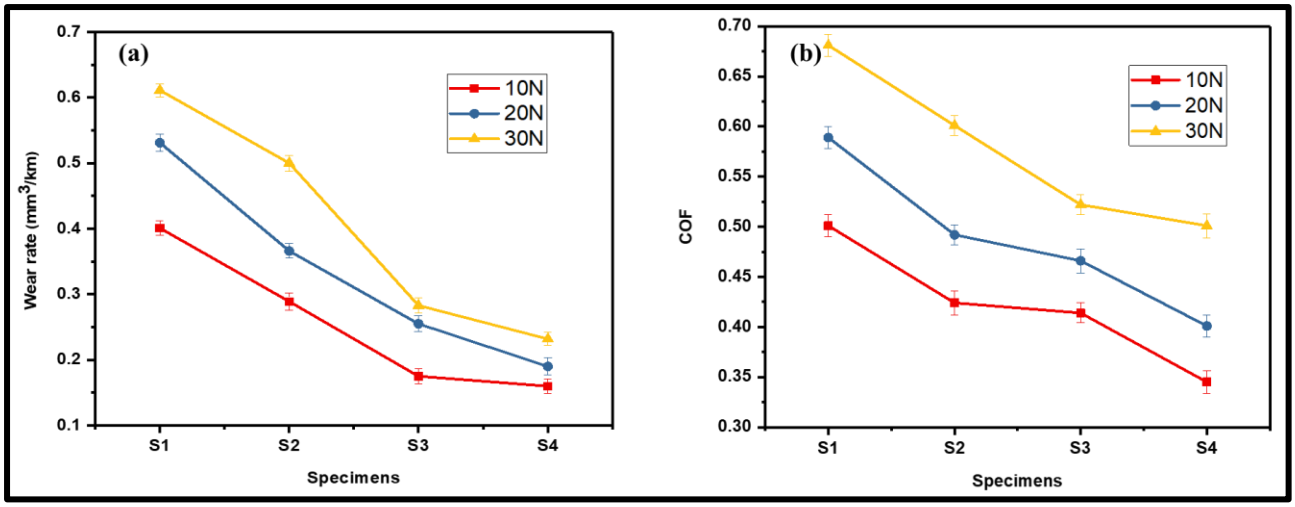


**Figure 6.4.** Influence of reinforcement on (a) wear rate and (b) COF at applied normal loads of 10, 20, and 30 N and sliding velocity of 2 m/s for a sliding distance of 2 km

### 6.2.3.2 Effect of applied normal load

The behaviour of the wear rate of the S1, S2, S3, and S4 specimens under various applied normal loads of 10, 20, and 30 N at a sliding speed of 2 m/s for a sliding distance of 2 km in dry sliding conditions is shown in Figure 6.5(a). At a sliding speed of 2 m/s, it is found that the average wear rate of S1, S2, S3, and S4 increases as applied normal stresses increase. Out of all the developed materials, the S1 exhibits the highest wear rate for all applied normal loads, and it also increases as the load increases. After some testing, a thin oxide layer will form and cover the surfaces of S1 during dry sliding. The formed oxide film keeps the S1 surface from making direct contact with the revolving counter disc surface since it is at a lower load that is insufficient to break such an oxide layer. As a result, the wear rate exhibits a lower value at lower applied normal loads, and wear is somewhat oxidative during this process. However, under higher applied normal loads, this produced oxide layer will quickly begin to deteriorate, exposing S1's new surface. under higher loads, this process will be ongoing, increasing the rate of wear. Furthermore, a higher applied normal load will also result in a higher contacting temperature, which increases oxidation and the formation of brittle oxide layers that are more susceptible to damage under higher applied loads. However, because of the wear resistance

created by the combined action of the SiC and graphite reinforcements in the matrix, the produced composites' wear rate decreases as the weight fraction of SiC and graphite increases. (Garg et al., 2024; Joshi et al., n.d.) state that although the wear rate of developed composite materials increases with applied normal load, it can be attributed to the breaking of oxidative layers and the pulling out of hard ceramic from the pin surface, which gets stuck between the mating surfaces and begins to act as a third body abrasion between the surfaces.

The fluctuation of COF with applied normal loads for developed materials S1, S2, S3, and S4 at a sliding speed of 2 m/s across a 2 km sliding distance in dry sliding conditions is shown in Figure 6.5(b). It is evident from the Figure that for all developed materials, the COF increases as the applied normal load increases. Out of all applied normal load situations, the produced material S1 shows the largest coefficient of variation (Cof). This is explained by the adhesive properties of tribo-contact, which cause the soft copper matrix to migrate in the direction of the harder countertop surface. As the applied load increases, more plastic deformation takes place, increasing the COF value. But in the designed composites, with higher applied normal loads, the tougher SiC particles can emerge out of the pin surface and raise the COF value.

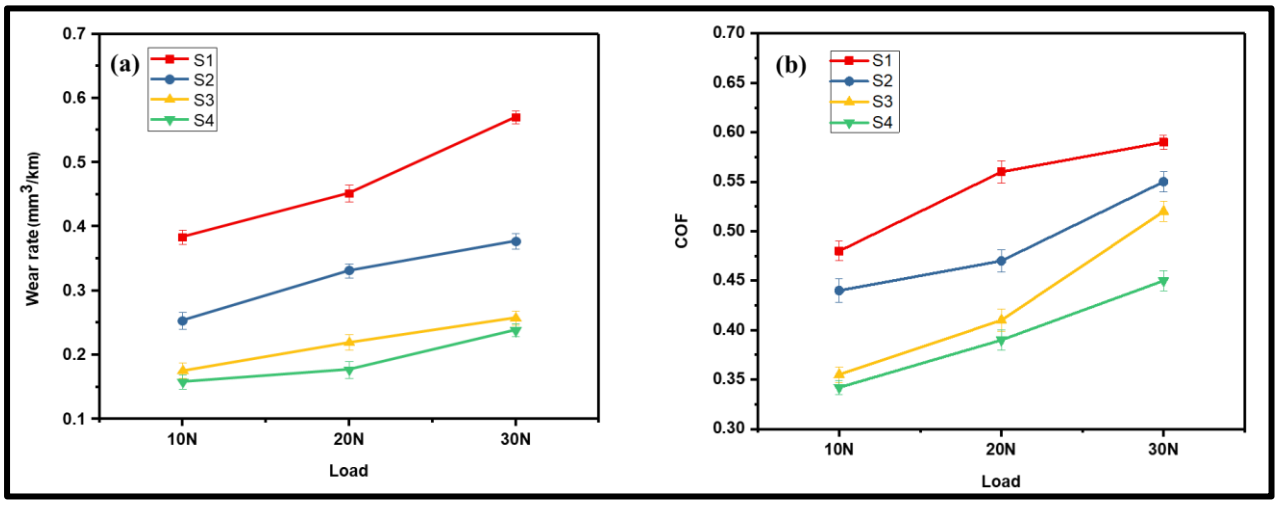


**Figure 6.5.** Effect of applied normal loads on (a) wear rate and (b) COF at a sliding velocity of 2 m/s for a sliding distance of 2 km

### 6.2.3.3 Effect of Sliding Speed

The impact of sliding speed at a sliding distance of 2 km, with an applied normal load of 30 N, on the wear rate of the produced materials S1, S2, S3, and S4 is shown in Figure 6.6(a). The Figure shows that, for the same applied normal load and sliding distance, the wear rate of all developed materials increases as the sliding speed increases from 1 m/s to 2 m/s. Additionally, at both sliding speeds of 1 and 2 m/s, it is shown that the S1 has the highest wear rate of all the developed materials. On the other hand, for both sliding speeds of 1 and 2 m/s, the produced composites exhibit a decreasing wear rate as the reinforcing content increases. The hybrid composites that have been created exhibit a higher wear rate at 2 m/s sliding speed as compared to 1 m/s wear at a sliding distance of 2 km and an applied normal load of 30 N. Thus, it can be said that, in dry sliding conditions, variations in sliding speed have a minor impact on the wear rate of all developed materials. At a sliding speed of 2 m/s, the S1 specimen exhibits a 22.9% higher wear rate than the S1 at a sliding speed of 1 m/s under an applied normal load of 30 N. Nonetheless, for the applied normal load of 30 N, the percentage increase in wear rate with the increase in sliding speed from 1 to 2 m/s is 59.4%, 48.4%, and 12.3% in the S2, S3, and S4 composites, respectively. The more reinforcing particles to be drawn out of the composites, such as the strained hardened copper particle, are responsible for this behaviour of an increase in wear rate of formed composites with an increase in sliding speed. This As a third body between the two mating surfaces, pulled-out and work-hardened hard particles are undoubtedly trapped between the contacting surfaces, increasing the wear rate from third body abrasion(Ankit et al., 2023).

The impact of sliding speed on coefficient of friction (Cof) of produced materials S1, S2, S3, and S4 is demonstrated in Figure 6.6(b) for a sliding distance of 2 km and an applied normal load of 30 N. According to the Figure, for a 2 km sliding distance under dry sliding conditions, the COF of developed materials increases as the sliding speed increases from 1 m/s to 2 m/s at

an applied normal force of 30 N. When the sliding speed increased from 1 m/s to 2 m/s at a normal load of 30 N, the COF for specimens S1, S2, S3, and S4 increased by 6.2%, 13.6%, 10.6%, and 15%, respectively. It is possible to explain this increase in COF in S1 with increasing sliding speed partly by the formation of a tougher oxide layer brought on by temperature increases at mating surfaces. The area of mating surfaces, that is, point contact, will be decreased by this hard surface. However, between the mating surfaces and the adherent layer formed in developed composite materials, the hard ceramic particles of SiC may mechanically comminute with the graphite particles, increasing COF.

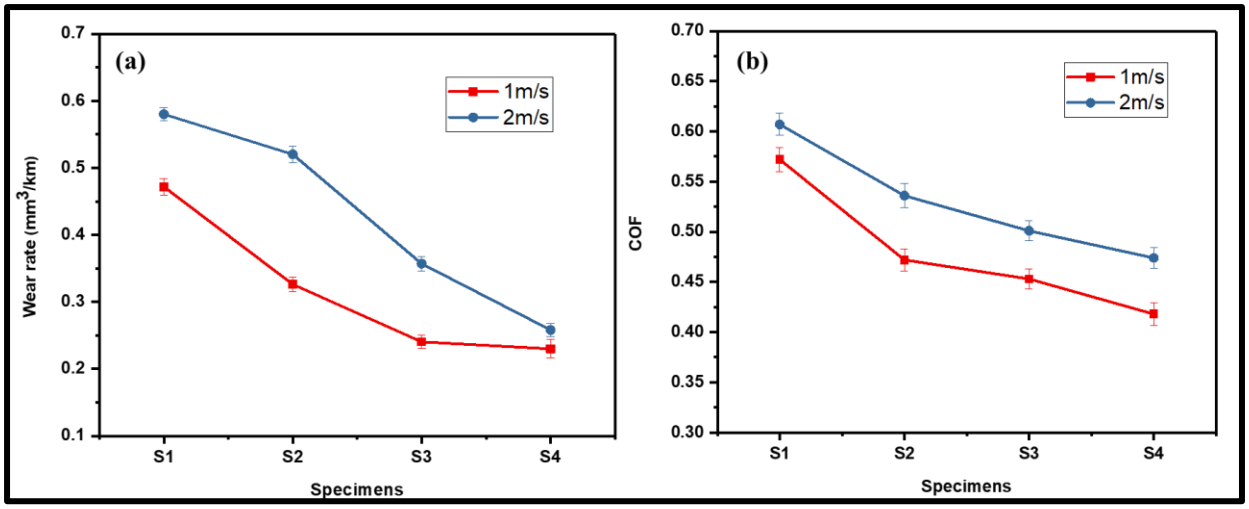


**Figure 6.6.** Effect of sliding speeds on (a) wear rate and (b) COF of developed materials at an applied normal load of 30 N for a sliding distance of 2 km

### 6.2.4 Analysis of Surfaces before and after deteriorated

#### 6.2.4 1. The deteriorated surface at a normal load of 30 N for all specimen

The SEM micrographs of the deteriorated surface of the specimen (S1) are shown in Figures 6.7(a) and 6.7(b), respectively, at a sliding distance of 2 km and sliding speeds of 1 m/s and 2 m/s under an applied normal load of 30 N. The SEM micrographs of the worn surface of the specimen (S2), however, are shown in Figures 6.7(c) and (d), where a normal load of 30 N is applied and the sliding distance is 2 km, with sliding speeds of 1 m/s and 2 m/s, respectively. As illustrated in Figure 6.7(a), the worn surface of the specimen (S1) specimen displays a

continuous, narrow groove at a sliding speed of 1 m/s and an applied normal force of 30 N. The severe delamination at a fast-sliding speed of 2 m/s at 30 N applied to a typical load is seen in Figure 6.7(b). This wear phenomenon was seen with the specimen (S1) at sliding speeds of 1 and 2 m/s. It was ascribed to the asperity of the hardened EN 30 counter steel disc, which resulted in severe abrasion and deep scratches to the surface of the pure copper. Consequently, as previously mentioned, pure copper specimens have a higher COF and wear rate than their composite counterparts. As illustrated 6.7(b), strong adhesion between the contacting surfaces at a greater sliding speed of 2 m/s causes a major delamination from the softer copper matrix(Ram Prabhu et al., 2014). As illustrated in Figures 6.7(c) and 6.7(d), respectively, the micrographs of the worn surfaces of the hybrid composite specimen (S2) reveal a delaminated layer and cracking in contrast to pure copper with an applied normal load of 30 N for sliding speeds of 1 and 2 m/s. This is explained by the lubricating properties of the graphite reinforcement, which provide smoother worn surfaces. Furthermore, the addition of SiC reinforcement to the copper matrix has increased hardness, which enhances wear resistance during dry sliding.

The SEM micrographs of the worn surface of the S3 are shown in Figures 6.7(e) and 6.7(f), respectively, at a sliding distance of 2 km and sliding speeds of 1 m/s and 2 m/s under an applied normal load of 30 N. On the other hand, the SEM micrographs of the specimen's (S4) worn surface with an applied normal load of 30 N for a 2 km sliding distance at sliding speeds of 1 m/s and 2 m/s, respectively, are shown in Figures 6.7(g) and 6.7(h). Figure 6.7(e) shows the specimen's worn surface with cracks at a low sliding velocity of 1 m/s, while Figure 6.7(f) shows the SiC particle smearing out at a high sliding velocity of 2 m/s. As SiC and graphite particle levels increased, the hybrid composite specimen (S4)'s worn surface, however, showed more variations in appearance, as seen in Figures 6.7(g) and 6.7(h). Smooth plough marks in the direction of sliding on the specimen's worn surface (S4) are seen in Figure 10(g).

Additionally, it exhibits indications of seamless ploughing, such as minute fractures, larger grains of deteriorated material, and the accumulation of an oxide layer. The study shows that when the amount of SiC and graphite reinforcement in the composite rises, the wear mechanism shifts from delamination to a combination of delamination and abrasion(Radhika et al., 2019). It is also noted that high-speed wear debris formation results in cracking. The copper matrix's hardness has been increased due to the higher concentrations of SiC and graphite. This can greatly boost the wear resistance of the matrix by preventing it from deforming when sliding throughout the counter surface.

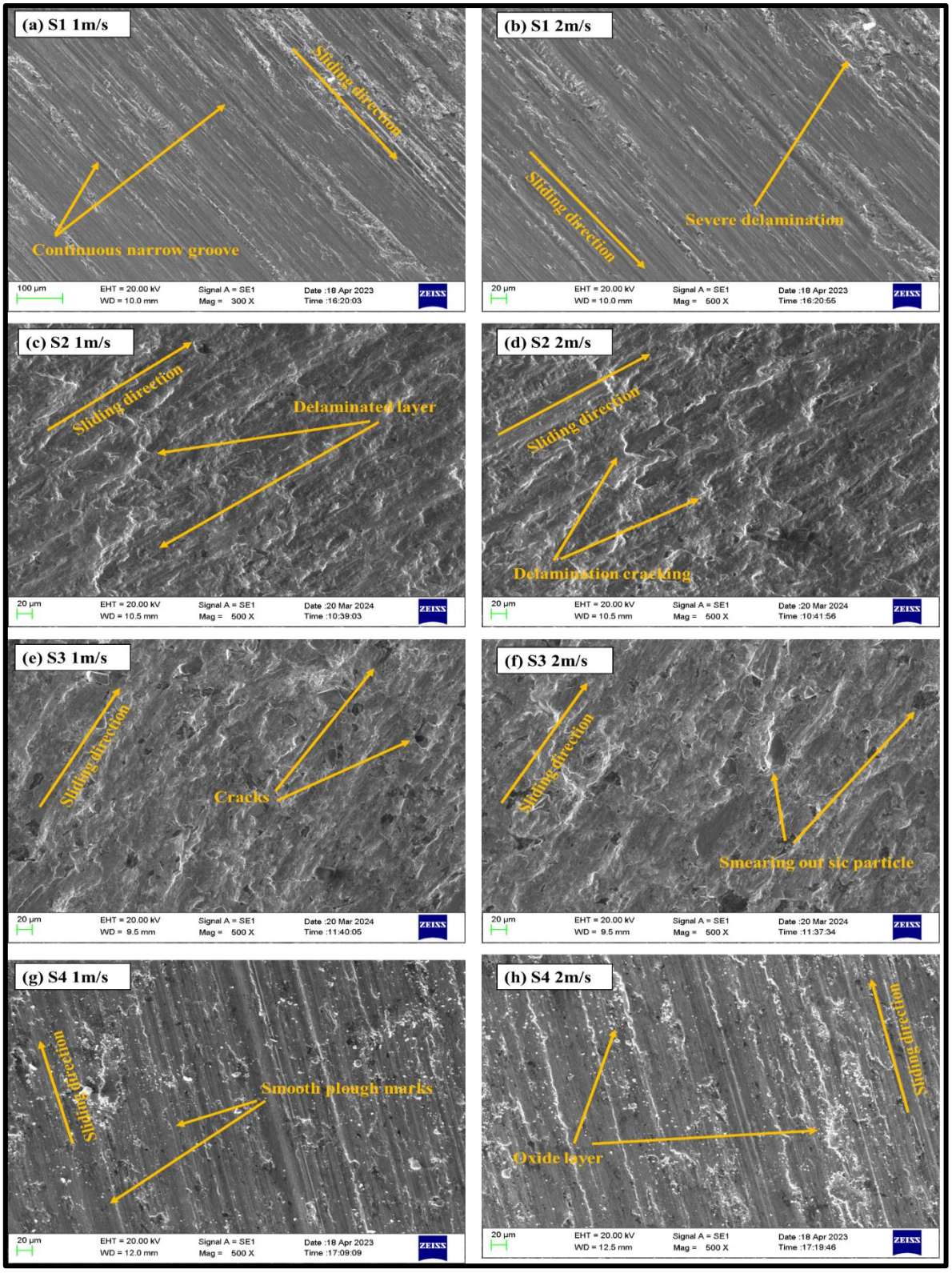


**Figure 6.7.** SEM micrograph of the worn surface at 30 N load for a sliding distance of 2 km of (a) S1, (c) S2, (e) S3, and (g)S4 at a sliding speed of 1 m/s and (b) S1, (d) S2, (f) S3, and (h) S4 at a sliding speed of 2 m/s.

### 6.2.4.2 EDS elemental color mapping and spectrum of the deteriorated surface at 30 N load

The EDS elemental colour mapping study is conducted to enhance the analysis of the worn surfaces of the produced composite and disclose its wear mechanism during the tribo-test. Figures 6.8(a) and 6.8(b) show the worn surfaces of S2 and their corresponding EDS elemental colour mapping. These measurements were taken at an applied normal load of 30 N, with a sliding distance of 2 km. The sliding speeds were 1 m/s and 2 m/s, respectively. The EDS elemental colour mapping of Cu, Cr, C, Si, O, and Fe is detected on the worn surface of S2 at sliding speeds of 1 m/s and 2 m/s, as shown in Figures 6.8(a) and 6.8(b). Therefore, it can be observed that the dry sliding tribo-test of the produced composite S2 involves the mechanisms of oxidative, abrasive, and adhesive wear. The addition of Cu, Cr, C, and Si elements in the colour mapping may be easily understand as they play a crucial role in the formation of composites. However, the presence of the element O can be attributed to the creation of oxides caused by the increase in temperature of the surfaces that are interacting under a higher applied normal stress of 30 N during the dry sliding tribo-test. However, the presence of Fe can be ascribed to the wearing of counter steel discs to a lesser extent when a higher applied force of 30 N is used during the dry sliding wear test. Figure 6.8(b) shows that the density of dots in the elemental colour mapping of C is greater when the sliding speed is 2 m/s compared to when it is 1 m/s. The occurrence can be ascribed to the initial contact of graphite particles at an elevated sliding velocity of 2 m/s and a perpendicular applied force of 30 N. However, it has been noticed that the concentration of dots in the elemental colour mapping of Fe is lower when the sliding speed is 2 m/s compared to when it is 1 m/s. The decrease in the appropriate contact between the surfaces can be ascribed to the increased sliding speed of 2 m/s.

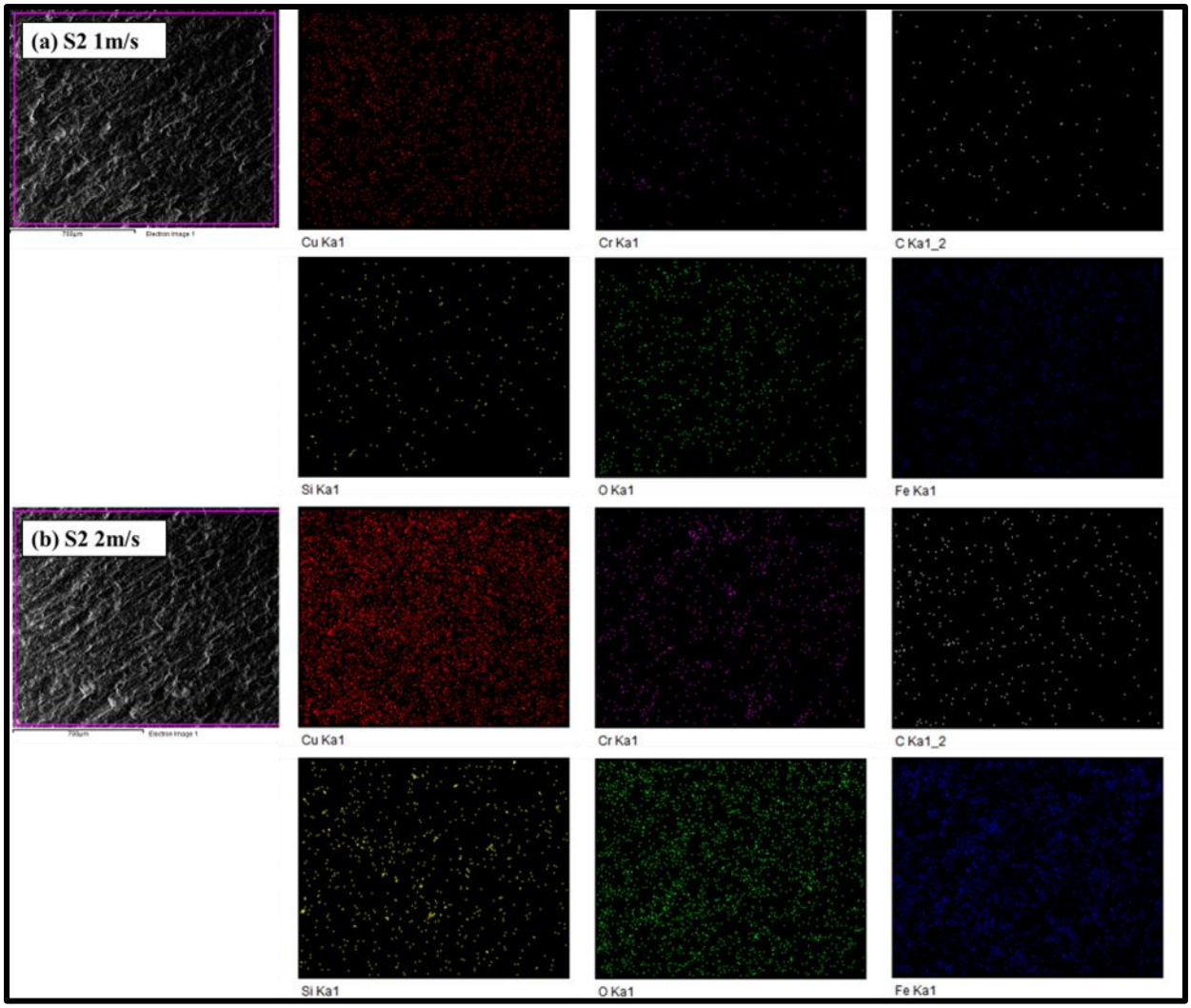


**Figure 6.8.** EDS elemental colour mapping of the worn surface of S2 at an applied normal load of 30 N for a sliding distance of 2 km

Figures 6.9(a) and 6.9(b) show the worn surfaces of S4 and its related EDS elemental colour mapping. These measurements were taken at an applied normal load of 30 N, a sliding distance of 2 km, and sliding speeds of 1 m/s and 2 m/s, respectively. The EDS elemental colour mapping of the deteriorated surfaces of the S4 specimen at sliding speeds of 1 m/s and 2 m/s reveals the presence of elements including Cu, Cr, C, Si, O, and Fe, as shown in Figures 6.9(a) and 6.9(b). The explanation for incorporating these factors into the mapping is same to what was previously described for Figure 6.8. Figure 6.9 shows that the density of carbon dots is similar in the colour mapping of the worn surface of S4 at both sliding speeds. This indicates

that the graphite layer in S4 is in a stable state, in contrast to the unstable graphitic state observed in the S2 specimen during the mapping analysis shown in Figure 6.8. Based on the examination of the colour distribution on the worn surface of S4, it can be concluded that the wear mechanisms of oxidation, abrasion, and adhesion are also present in S4.

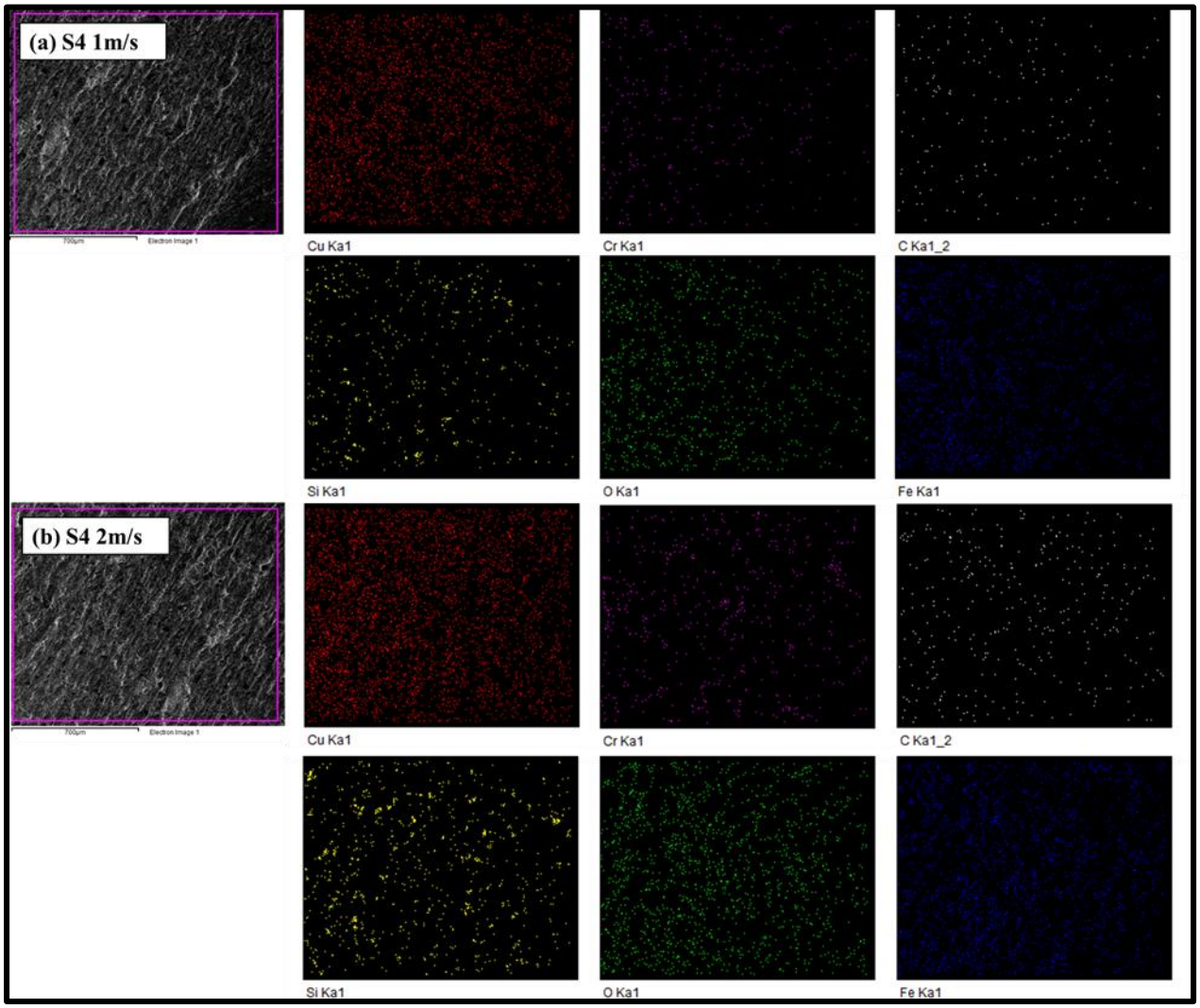


**Figure 6.9.** EDS elemental colour mapping of the worn surface of S4 at an applied normal load of 30 N for a sliding distance of 2 km

### 6.2.5 Atomic force microscopy (AFM) analysis of deteriorated surfaces

Figures 6.10(a), 6.10(c), and 6.10(e) show the 3D images of worn surfaces of the produced materials S1, S2, and S4, respectively, obtained using atomic force microscopy (AFM). The images were captured under the conditions of a sliding speed of 1 m/s, an applied normal load

of 30 N, and a sliding distance of 2 km. Figures 6.10 (b), 6.10 (d), and 6.10 (f) show the 3D pictures of worn surfaces of the produced materials S1, S2, and S4, respectively, obtained using an atomic force microscopy (AFM). The measurements were taken at a sliding speed of 2 m/s and an applied normal load of 30 N, with a sliding distance of 2 km. Scanning probe microscopy is very suitable for evaluating the surface roughness and micro-texture of worn surfaces in produced materials. For the atomic force microscopy (AFM) analysis, a depth of 50 μm from the worn surface of the generated materials is taken into account. Figures 6.10 (a) and 6.10 (b) clearly demonstrate that the peak values of the worn surface of S1 at a sliding speed of 2 m/s are greater than the peak values of the worn surface of S1 at a sliding speed of 1 m/s. This indicates that the rate of material wear is higher at higher sliding speeds. The peak value of worn surfaces of S2 also follows a similar pattern, as depicted in Figures 6.10 (c) and 6.10 (d). Nevertheless, the AFM micrograph of S4 reveals a similar level of peak value for the worn surface at sliding speeds of 1 m/s and 2 m/s, as depicted in Figures 6.10 (e) and 6.10 (f). However, it is worth noting that the wear loss is greater at sliding speeds of 2 m/s compared to the loss at sliding speeds of 1 m/s, as previously reported. Figure 6.10 shows that the peak value intensity of the worn surfaces in the composite material is lower than the peak value intensity of the copper matrix, regardless of the sliding speed (1 m/s or 2 m/s). This indicates that the wear loss in the composites is lower than in their matrix.

Table 6.2 displays the mean roughness (Ra) and root mean square roughness (Rq) of the initial and worn surfaces of the produced materials S1, S2, and S4. These measurements were taken under a normal load of 30 N and sliding speeds of 1 m/s and 2 m/s, with a total sliding distance of 2 km. Table 6.2 demonstrates that the initial roughness value of the samples is lower than the roughness value after wear. When the sliding speed increases from 1 m/s to 2 m/s, the average roughness (Ra) of S1, S2, and S4 increases from 0.350 μm, 0.136 μm, and 0.1309 μm to 0.421 μm, 0.298 μm, and 0.1821 μm, respectively.

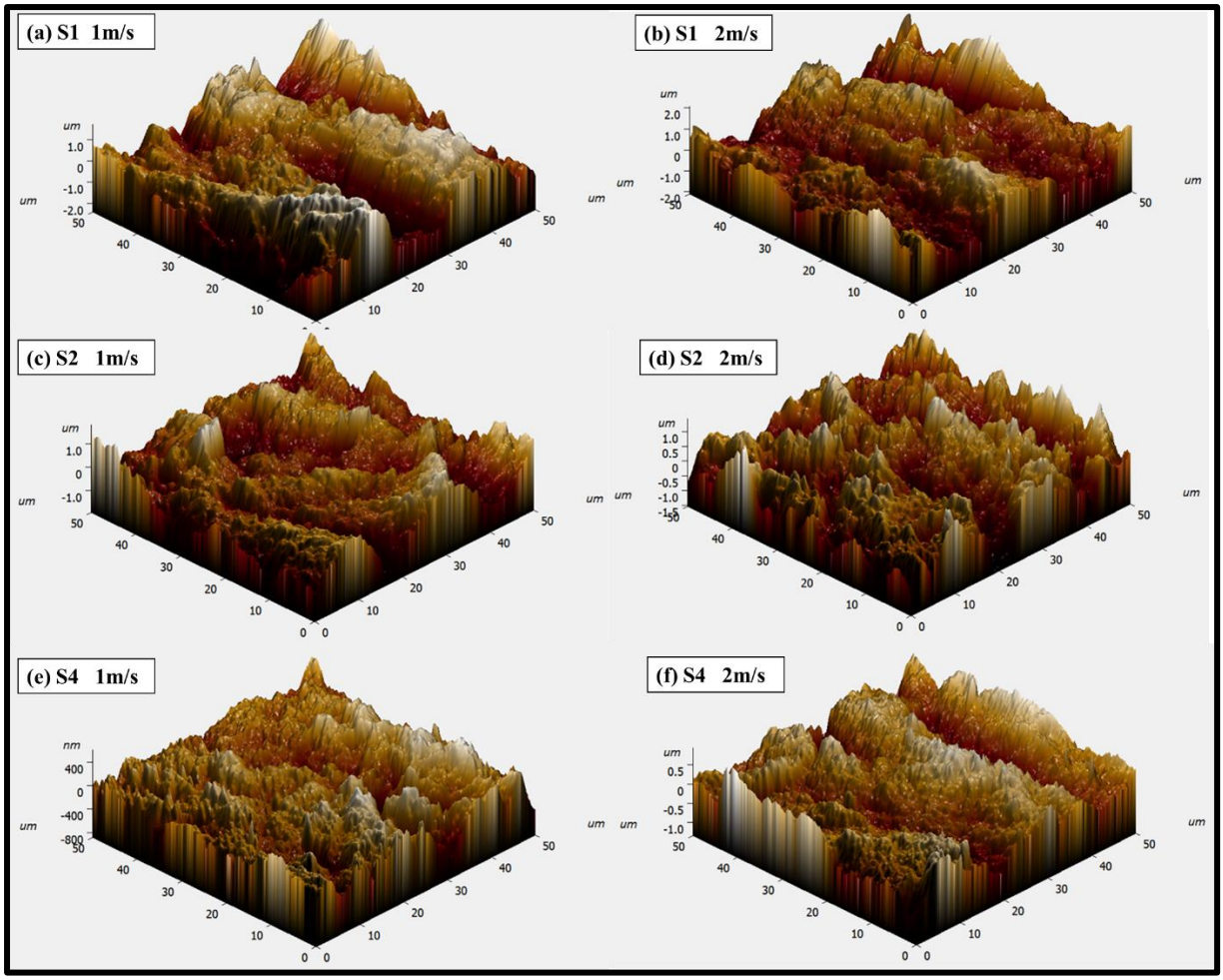


**Figure 6.10.** Atomic force microscopy (AFM) 3D morphology of the worn surfaces at an applied normal load of 30 N for a sliding distance of 2 km

Table 6.2 demonstrates that the root mean square roughness (Rq) has an equivalent result. Both at sliding speeds of 1 m/s and 2 m/s, the S4 specimen exhibited the lowest surface roughness (Ra), providing further evidence that the S4 specimen has the least amount of wear loss.

**Table 6.2.** Surface roughness parameters of before and after wear of the developed materials at an applied normal load of 30 N for a sliding distance of 2 km.

| **Parameters** | **S1 (1m/s)** | **S1 (2m/s)** | **S2 (1m/s)** | **S2 (2m/s)** | **S4 (1m/s)** | **S4 (2m/s)** |
|---|---|---|---|---|---|---|
| Average roughness Ra (μm) | 0.350 | 0.421 | 0.136 | 0.298 | 0.1309 | 0.1821 |
| Root mean square roughness Rq (μm) | 0.436 | 0.560 | 0.198 | 0.321 | 0.1634 | 0.2167 |

The AFM test results are consistent with the SEM findings obtained from different sliding speeds mentioned earlier.

### 6.3 Conclusion

Copper composites, namely S2, S3, and S4, as well as unreinforced copper (S1), were effectively made utilizing the powder metallurgy technique. The experimental study has been conducted to evaluate their mechanical, physical, and tribological properties. The microstructural investigations verify the even dispersion of reinforcing particles inside the copper matrix throughout the sintering process. The primary finding of this study can be briefly stated as follows:

1) The scanning electron microscopy (SEM) analysis of composites reveals the presence of reinforcing particles distributed evenly and uniformly throughout the matrix. An accumulation is evident when the amount of reinforcement is increased. Energy dispersive x-ray spectroscopy (EDS) elemental colour mapping can accurately identify and display the various reinforcements inside the copper matrix.
2) The density of the composites drops as the weight percentage of silicon carbide (SiC) and Gr in the copper matrix increases because silicon carbide (SiC) and Gr have a lower density than copper, reinforcing the composites' lower density. Enhancing the concentration of reinforcement results in a corresponding increase in the porosity of the composite material.
3) The inclusion of silicon carbide (SiC) and graphite significantly improved the hardness of the produced composites compared to their matrix. The hardness of the copper matrix increases strongly with the addition of 6 wt.% of silicon carbide (SiC) and graphite (Gr) reinforcement. However, after this point, the hardness diminishes, although it remains higher than the matrix alone. The highest hardness level recorded in S3 is 93.6 HV, representing a significant enhancement of 60.36% compared to pure copper (56.5 HV).

4) It has been discovered that the wear rate and COF of composites decline as the reinforcing wt.% increases. At a reinforcing component concentration of 9wt.%, the wear rate is minimized due to the combined influence of graphite (Gr) and silicon carbide (SiC) particles. The inclusion of graphite minimizes wear using its inherent self-lubricating characteristic. Therefore, including graphite (Gr) in metal matrix composites (MMCs) gives the composites a self-lubricating material characteristic.
5) Examining the deteriorated surfaces indicates that the principal wear mechanism for pure copper specimens is either adhesion or delamination. silicon carbide (SiC) and graphite (Gr) reinforced composites revealed a combination of wear mechanisms, including adhesive, abrasive, oxidative, and delamination wear modes.